Author/s:
Hendrikse, SIS;Todorova, N;Soleimaninejad, H;Charchar, P;Sani, M-A;Al Taief, K;Berengut, JF;Wickham, SFJ;Gras, SL;Fahrenbach, AC;Thordarson, P;Ellis, AV

Title:
Exploring Artificial Nucleic Acid Mimicking Peptide Nanofibers

Date:
2023-05-17

Citation:
Hendrikse, S. I. S., Todorova, N., Soleimaninejad, H., Charchar, P., Sani, M. -A., Al Taief, K., Berengut, J. F., Wickham, S. F. J., Gras, S. L., Fahrenbach, A. C., Thordarson, P. & Ellis, A. V. (2023). Exploring Artificial Nucleic Acid Mimicking Peptide Nanofibers. CHEMISTRY OF MATERIALS, 35 (11), pp.4355-4365. https://doi.org/10.1021/acs.chemmater.3c00445.

Persistent Link:
https://hdl.handle.net/11343/332876

Exploring artificial nucleic acid mimicking peptide nanofibers

Simone I. S. Hendrikse,[*1,2] Nevena Todorova,[3] Hamid Soleimaninejad,[4] Patrick Charchar,[3] Marc-Antoine Sani,[5] Karrar Al Taief,[2,6,7] Jonathan F. Berengut,[8,9] Shelley F.J. Wickham,[8,9,10] Sally L. Gras,[1,11] Albert C. Fahrenbach,[2,7] Pall Thordarson,[2,6,7] Amanda V. Ellis[1*]

1 Department of Chemical Engineering, The University of Melbourne, Melbourne, VIC 3010, Australia

* E-mail: shendriksela@unimelb.edu.au, amanda.ellis@unimelb.edu.au

2 School of Chemistry, University of New South Wales, Sydney, NSW 2052, Australia

3 School of Engineering, RMIT University, Melbourne, Victoria 3001, Australia

4 Biological Optical Microscopy Platform (BOMP), The University of Melbourne, Parkville, VIC 3010, Australia

5 School of Chemistry, Bio21 Institute, University of Melbourne, Melbourne, Victoria 3010, Australia

6 Australian Centre for Nanomedicine, University of New South Wales, Sydney, NSW 2052 Australia

7 The UNSW RNA Institute, University of New South Wales, Sydney, NSW 2052, Australia

8 School of Chemistry, University of Sydney, Sydney, NSW 2006, Australia

9 The University of Sydney Nano Institute, University of Sydney, Sydney, NSW 2006, Australia

10 School of Physics, University of Sydney, Sydney, NSW 2006, Australia

11 Bio21 Molecular Science and Biotechnology Institute, University of Melbourne, Melbourne, Victoria 3010, Australia

ABSTRACT: Nucleic acids play key roles in Nature, including the storage of genetic information and the translation into a wide variety of proteins that collectively build up cells. Their intrinsic programmability can be utilized to bind specific targets for a wide variety of biomedical applications. However, naturally derived nucleic acids are susceptible to degradation and their large-scale synthesis is costly. Although artificial polymeric nucleic acids show great promise, they are typically more flexible, and therefore their secondary structure hard to control. Here, we designed polymerizable monomers that upon free-radical polymerization were able to form micrometer-long fibrous structures containing mononucleotide grafts. These fibers were a direct result of predesigned non-covalent interactions along the polymer backbone supported by the inclusion of peptide linkers installed between polymerizable headgroups and mononucleotides. The resulting hybrid nucleic acid-peptide homopolymers exhibited secondary structure signatures analogous to natural RNA but were unfolded and fibrous in morphology, in contrast to the collapsed globular structures typically observed for natural RNA in water. The peripheral exposed mononucleotides showed capacity to engage in complementary binding to both 1D and more complex 3D nucleic acid structures, showing potential to be utilized as templates for biomedical applications.

Built of only four distinct repeatable units, strands of deoxynucleic acids (DNA), stored in cellular nuclei, encode for all the genetic information that sustains life.[1, 2] Next to the remarkable ability to be translated into all proteins present in cells, its predictable Watson-Crick-Franklin base pairing enables reliable binding of targets with extremely high precision. RNA displays many structural similarities to DNA, *e.g.*, the phosphodiester backbone, carbohydrate (ribose instead of deoxyribose) and four distinct nucleobases (containing uracil instead of thymine). In contrast to DNA, RNA mainly exists as a single stranded polymer able to translocate genetic information from the nucleus across the cell, and can form complex secondary structures allowing binding to specific receptors. However, RNA is less stable than DNA due to the extra 2'-hydroxyl group present at the ribose carbohydrate.[3] Using natural or modified DNA or RNA opens up a variety of applications, including in the study of fundamental processes *in vivo*, such as disease progression, the ability to alter cellular processes, gene therapy, immunity engineering or drug delivery, and as probes for biosensing and disease diagnosis.[4-6]

Despite the remarkable properties of nucleic acids, they suffer from poor stability. This instability is due to their folding and binding being dependent on high salt concentrations, typically much higher than is physiologically relevant.[7] Moreover, the (organic) synthesis of micrometer long synthetic nucleotide sequences on the milligram-to-gram scale is difficult to achieve. For decades, researchers have been exploring different ways to stabilize, manipulate and create nucleic acid mimics aiming to unveil their full potential for a wide variety of applications.

Approaches range from introducing small modifications within the backbone or nucleobase,[8] to hybrid DNA grafted polymers,[9] artificial foldamers[10] and nucleobase-functionalized polymers.[11] In particular, peptide nucleic acids (PNAs), discovered in the early 1990s, have shown great potential.[12] Since PNAs do not include phosphate in the backbone, the absence of charge endows the molecule with high binding affinity towards DNA, resulting in stronger binding compared to the DNA/DNA interactions present in DNA duplex formation. PNAs, however, are very short in length (about 15-20 nucleobases), and aside from containing nucleobases, they do not display other characteristic features of DNA and RNA (phosphates and (deoxy) riboses). Also, despite their high stability and resistance against nucleases and proteases, their circulation time *in vivo* is only a few minutes, similar to unmodified oligonucleotides.[13] Additionally, the intrinsic hydrophobic nature of PNAs is prone to form globular structures and large aggregates, as well as non-sequence-specific binding.[14]

The iterative synthesis of sequence-controlled molecules, *i.e.*, utilized during the synthesis of synthetic DNA, RNA and PNAs,[15, 16] typically results in restricted polymer lengths due to the accumulation of near complete yields and side product formation (such as deletion sequences). Polymerization strategies that have been used to address this limitation include living radical polymerization techniques, such as reversible addition fragmentation chain transfer (RAFT) and atom transfer radical polymerization (ATRP).[11] This approach allows the fabrication of DNA-grafted polymers with various architectures, displaying oligonucleotide blocks in a linear or branched fashion.[17] The resulting block-co-polymers produced in this way follow similar self-assembly rules as 2D materials, in which the packing parameter dictates the subsequent shape they form.[18] However, the intrinsic negative charges situated on the phosphates can create collective repulsion and polymeric collapse into densely packed and globular structures that likely display limited complementary binding capacity even when a high salt concentration is used. To prevent such collapse and allow pre-alignment for optimal binding, simultaneous tuning of the molecular structure, polymerization strategy, and assembly protocol is required. For example, DNA bottlebrushes[19] and the self-assembly of amphiphilic DNA polymers into fibrous DNA brushes have been developed.[20, 21] Similar to spherical nucleic acid nanoparticles,[22] the high density of oligonucleotides displayed on these polymers is expected to enhance the performance in *e.g.*, biosensing and gene regulatory applications due to gained avidity, though DNA-grafted polymers still suffer from drawbacks, such as low synthesis yields and only small DNA block lengths.[9, 23]

Although the native DNA, and also RNA, molecular structure is able to fold in double helical or complex tertiary structures (such as the coaxial stacking in tRNA), such control over the folding of simple artificial polymers with pendent mononucleotides is hard to achieve due to the inherent flexibility of the polymeric backbone and a lack of non-covalent interactions that could aid in supramolecular folding. Here, we have developed a simple polymerization platform to create micrometer long and fibrous nucleic acid mimicking polymers using free-radical polymerization. Both DNA and RNA mimicking homopolymers were synthesized and their self-assembly was investigated using a variety of experimental techniques (including spectroscopy, scattering, and microscopy) and computational molecular dynamics simulations. The synthesized hybrid polymers assembled into fibrous morphologies in aqueous solutions facilitated by non-covalent interactions lateral to the polymeric backbone. This enabled the formation of pre-organized fibers that supported transient interactions with complementary native and natural RNA and DNA.

RESULTS AND DISCUSSION

Molecular design and synthesis. Radical polymerization is a powerful technique to synthesize polymers with repeated units.[24] Although a controlled length can be obtained when a chain transfer agent is used — *e.g.*, during RAFT polymerization[25] — much longer polymer chains can be achieved, containing over thousand repeats, in an uncontrolled fashion. However, there is a play-off between length and polydispersity of the final polymer product. Moreover, the molecular structure as well as the solvent choice can influence polymerization reactivity and hence the outcome. Here we employed uncontrolled free-radical polymerization to achieve nucleic acid mimicking polymers that are micrometers in length.

Grafting mononucleotides directly to the polymeric backbone might result in a polymeric collapse into packed structures in an aqueous solution, due to the collective repulsive forces between the negatively charged phosphate groups that are present in the lateral mononucleotides and might create limitations for complementary binding. To support a fibrous-like morphology, we introduced a short peptide linker between the methacrylate and mononucleotide (Scheme 1) to encourage additional non-covalent interactions to form. Non-covalent interactions, such as hydrogen bonds and hydrophobic interactions, can overcome the negative repulsive forces by stabilizing the polymeric backbone in the lateral direction.

Hydrophobic amino acids were considered for the peptide linker design to create a substantial hydrophobic pocket that would encourage a hydrophobic collapse, thereby protecting the inner non-covalent bonds from water penetration and interference. The most utilized amino acid in short peptide self-assembly is phenylalanine (*e.g.*, in Fmoc-FF[26]), due to its ability to form strong π–π interactions between adjacent aromatic rings. In this instance, non-aromatic amino acid alanine was selected for use in the peptide linker design as the absorbance of phenyl rings (due to the inclusion of phenylalanine) overlaps with nucleic acid absorption (at around 260 nm[27]), thereby complicating spectroscopic observations. Moreover, the short methyl side-chain of alanine is anticipated to reduce steric hindrance between adjacent side-chains. As such, the following spacer design was chosen for this study: a peptide linker containing two alanine residues to ensure a hydrophobic pocket; a flexible glycine to provide spacing and bond rotation; and a threonine onto which a mononucleotide could be installed (AAGT). A modular synthesis platform was developed to fabricate artificial DNA

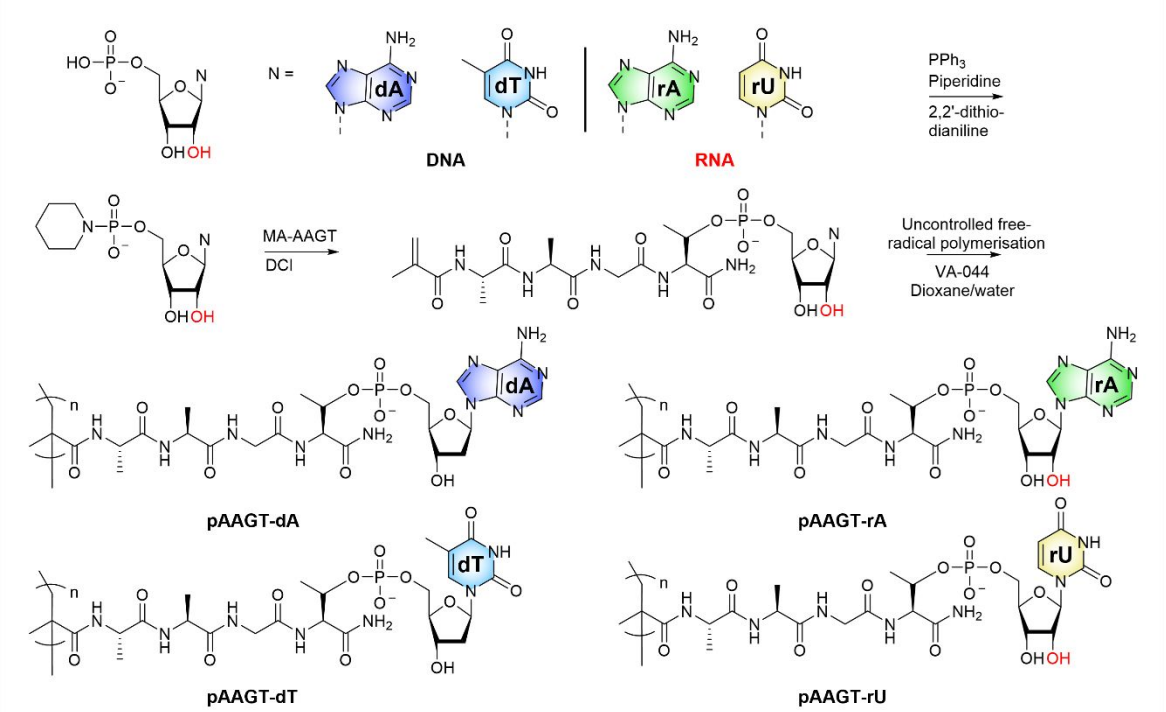

Scheme 1. Synthesis of homopolymeric DNA and RNA mimics. DNA and RNA mononucleotides adenine (A), thymine (T, only DNA) and uracil (U, only RNA) were pre-activated with piperidine prior to coupling to a methacrylated peptide linker MA-AAGT. The obtained monomers were then polymerized using the radical initiator VA-044 for 2 h, at elevated temperature, to afford the homopolymers pAAGT-rA, pAAGT-rU, pAAGT-dA and pAAGT-dT (r indicates RNA and d indicates DNA).

(pAAGT-dN, N=nucleotide) and RNA (pAAGT-rN) homopolymers displaying the mononucleotides adenine (dA or rA), uracil (rU) or thymine (dT) (r indicates RNA and d indicates DNA, Scheme 1).

DNA and RNA mononucleotides were first activated with piperidine prior to coupling to an N-terminal methacrylated peptide linker (MA-AAGT). Commencing with either DNA or RNA mononucleotides (rA, dA, rU or dT, 5'-monophosphates, where r indicates RNA and d indicates DNA), both DNA and RNA mimicking homopolymers were obtained by uncontrolled free-radical polymerization. The water-soluble initiator VA-044[28] was utilized to generate radicals at elevated temperature and initiate the radical polymerization reaction in a mixture of dioxane/water to disrupt potential non-covalent interactions between side-chains. After 2 h at 80 °C, the reaction was quenched in liquid nitrogen and the mixture was dialyzed against water. Lyophilization afforded the homopolymeric peptide–nucleotides. The polymers obtained were characterized using proton ^{1}H and phosphorus ^{31}P solution NMR (SI, see synthetic procedures), and several spectroscopic, scattering, and microscopic techniques (see below and SI). Due to the inherent charges, characterization using gel permeation chromatography (GPC) to obtain a number average molecular weight estimate was unsuccessful as the polymers interacted strongly with the column (SI, GPC chromatogram section). Matrix assisted laser desorption/ionization (MALDI) confirmed polymeric species and dynamic light scattering (DLS) the existence of aggregated structures (SI, MALDI and DLS, respectively).

As proof-of-concept, a cytosine dC polymer was also synthesized. It should be noted that cytosine- and guanine-rich sequences typically adopt complex secondary structures including i-motifs[29] and G-quadruplexes,[30] respectively, and therefore might form complex secondary structures. These types of structures were likely apparent during the nucleotide activation, in which organo gels quickly formed with only a low or negligible amount of the desired activated nucleotide species.

Homopolymers contain non-covalent interactions between lateral side-chains. First, the assembly and internal order of the individual DNA and RNA mimicking homopolymers was investigated in water using CD and UV spectrophotometry. To reduce kinetically trapped structures, the samples were briefly heated to 80 °C for 5 min and subsequently allowed to cool to room temperature, followed by overnight equilibration prior to analysis.

As a control, the polymeric peptide without any mononucleotides attached was used. The control polypeptide (pAAGT) showed a negative Cotton band at approximately 190 nm in the CD spectra (SI, Figure S1A). To investigate whether a free tetrapeptide sequence is capable of facilitating supramolecular self-assembly in the lateral direction, and omitting the influence of a covalent linkage, *i.e.*, stacking of tetrapeptides as a result of non-covalent interactions rather than covalent bond fixation, the peptide sequence AAGS was investigated in CD as well. Comparing this free peptide sequence AAGS to polymeric pAAGT revealed a lower stability at elevated temperatures (SI, Figure S1B). This might indicate that there are weak lateral non-covalent interactions present, though, are easily broken as compared to a stable covalent reinforcement. Both CD curves resembled a random coil conformation

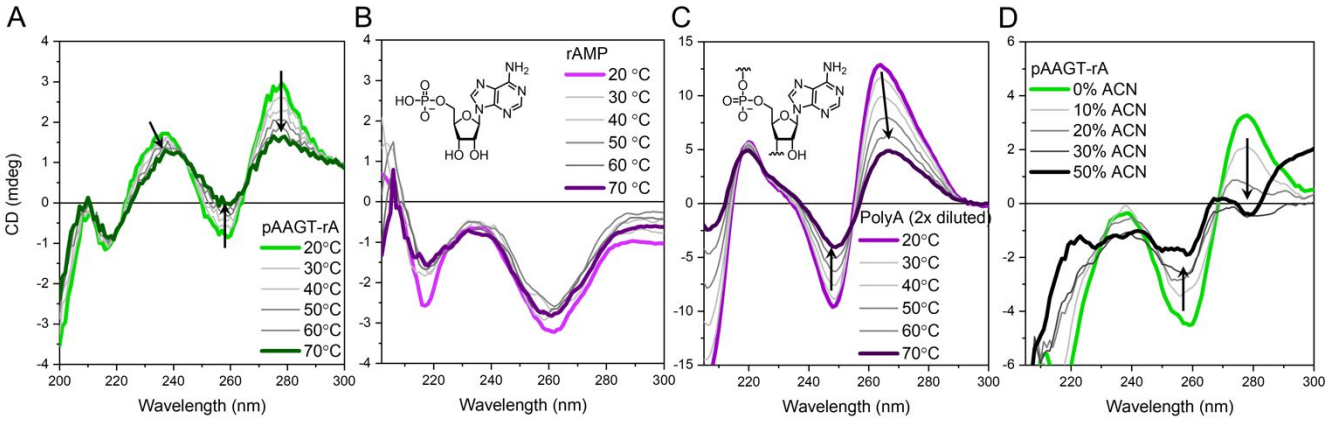

Figure 1. Circular dichroism studies of the artificial homopolymer pAAGT-rA (A and D) as compared to free mononucleotide adenine (rAMP, B) and native PolyA (C). CD spectra are depicted with variable temperatures (A-C) or acetonitrile (ACN) content (D). Spectra (B) and (D) are 10 points smoothed for clarity. λ = 1 mm and c = 0.35 mg mL^{-1} in 10 mM phosphate buffer including 100 mM NaCl (pH7) or λ = 10 mm and c = 0.035 mg mL^{-1} in water or water/acetonitrile (D).

found in proteins rather than α-helical or β-sheet arrangements.[31] This suggests that the lateral peptide side-chains may only adopt very weak non-covalent interactions that are unable to support ordered structures (such as an α-helix or β-sheet), arising from asymmetric amplification of hydrogen bonding between stacked lateral amides (hence preference for helicity). The reinforcement of the covalent backbone might also hamper optimal lateral peptide stacking and ordered secondary structures to form. Nevertheless, the absence of CD and UV (SI, Figure S1A) signals above 200 nm in the peptide polymer pAAGT enables the investigation of non-covalent interactions between nucleic acids in the next step (*i.e.*, in the nucleic acid homopolymers), that are expected to occur around 260 nm.[27]

The synthesized peptide-DNA and peptide-RNA homopolymers were first investigated by UV and CD while comparing to the free monomeric nucleotides and commercially available natural polynucleotides (polyadenylic acid, PolyA and polyuridylic acid, PolyU). Note that in contrast to natural polynucleotides that have the mononucleotides connected *via* their phosphate backbone, the peptide–nucleotide grafts can freely rotate around the polymer axis as they are only connected at the end of the peptide linker, enriching them with more flexibility. All DNA and RNA mimicking homopolymers showed distinct CD signals, in combination with similar absorbance maxima around 260 nm (SI, Figures S2–S5). The RNA artificial polymers showed a slightly higher CD signal, as compared to their DNA equivalents, despite having additional hydroxyl groups at the 2'-location in the ribose (SI, Figure S2). In particular, the artificial homopolymer pAAGT-rA (RNA adenine) displayed a substantial CD signal.

Figure 1 (and SI, Figure S3) shows a comparison of pAAGT-rA (RNA adenine, Figure 1A) with mononucleotide adenine (rAMP, Figure 1B) and native PolyA (Figure 1C). A distinct CD spectrum was not expected for mononucleotide rAMP (Figure 1B), because of repulsive electrostatic interactions that discourage intermolecular non-covalent interactions, and hence supramolecular self-assembly, to occur. In practice, AMP shows a slight CD effect, possibly arising from its rotation relative to the (deoxy)ribose.[32] The lack of an observable temperature responsiveness further confirms a lack in supramolecular assembly. In contrast, pAAGT-rA (Figure 1A) did show a distinct CD spectrum, significantly different from rAMP, potentially indicating the existence of directional non-covalent interactions. The pAAGT-rA spectrum was also strikingly similar to the spectrum of native PolyA (Figure 1C). However, the CD intensity was significantly lower, and the maxima and minima bands were slightly shifted (Figure 1A vs 1C, and Figure S2-S3). Both pAAGT-rA (Figure 1A) and native PolyA (Figure 1C) displayed gradually decreasing CD intensities upon increasing temperature. This temperature responsiveness indicates a slight change in morphology, which is likely due to the gradual disruption of non-covalent interactions between the lateral monomers (such as nucleobase-nucleobase interactions) upon increasing temperature. In contrast, the artificial homopolymer uracil (pAAGT-rU) and native PolyU remained stable upon increasing temperature, with only modest changes observed in the CD spectra (SI, Figure S4), indicating a potential lack of non-covalent interactions between lateral uracil nucleotides within these polymers.

To investigate whether the non-covalent interactions originate from lateral nucleotide–nucleotide interactions (hydrogen bonds between the carbohydrates and/or π–π between adjacent nucleobases), a "good" solvent (acetonitrile, ACN) was gradually added to increase the solvation of the slightly hydrophobic nucleobases. Upon increasing acetonitrile content any non-covalent interactions present are disrupted evidenced by a change in CD signal. Indeed, upon the addition of ACN to pAAGT-rA (Figure 1D), the CD signal arising from the nucleotides decreased and more closely resembled the free monomeric rAMP (Figure 1B), whereas the CD signal arising from the peptide backbone remained similar. This observation confirms the existence of lateral interactions between nucleobases in water.

Additionally, the influence of salt on the secondary structures was examined. Salt was found to have a negligible influence on the secondary structure of the polymers since both the CD and UV spectra of the

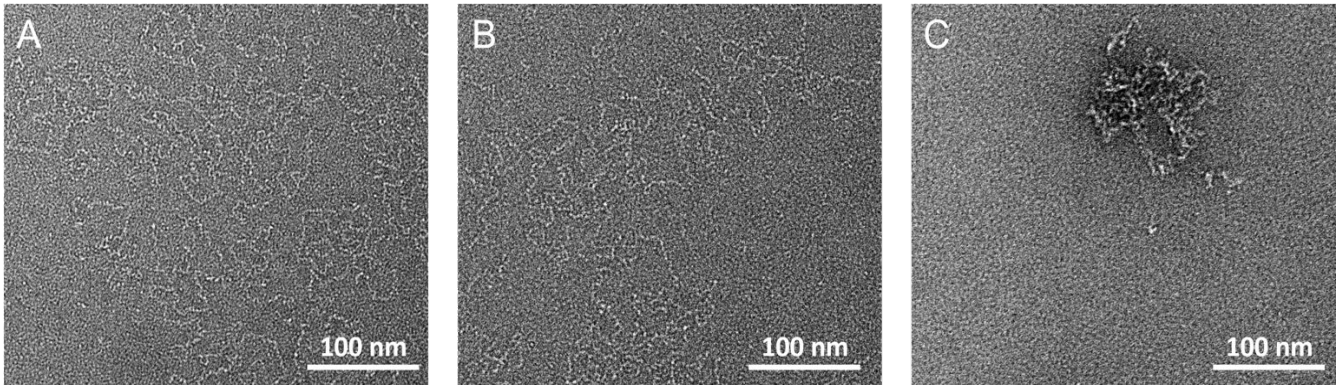

Figure 2. TEM images of pAAGT-rA (A), pAAGT-rU (B) and native polyA (C). All samples were 0.25 mg mL^{-1} in water and negatively stained with 2% uranyl acetate.

homopolymers dissolved in either water or phosphate buffer (with 100 mM NaCl) were similar (SI, Figure S6).

Taking all the CD results together, lateral assembly of the structures, in particular pAAGT-rA, and to the lesser extent in the other variants, was evidenced by: (1) a significantly different CD profile relative to free monomeric nucleotide, (2) a gradual decrease in CD signal upon increasing temperature indicating morphology changes, and, (3) lateral nucleotide–nucleotide interactions were disrupted in organic solvent (ACN). The reduced intensity of the CD signal and the shift in Cotton bands, compared to native poly-RNA, suggests reduced order and potentially a decrease in pitch length. The slightly lower CD signal of the DNA polymers compared to their RNA equivalents underpins the importance of stereochemistry in supramolecular self-assembly. The influence of the carbohydrate stereochemistry has previously been demonstrated to influence supramolecular packing and subsequently the helicity.[33, 34]

Homopolymers assemble into fibrous structures. Scattering and microscopy techniques were employed to assess the morphology of the structures formed by the different homopolymeric variants as compared to native polyA. Negative stained transmission electron microscopy (TEM) revealed fibrous structures approximately 4 nm in diameter for both RNA and DNA artificial homopolymers (Figure 2A and B, and SI, Figure S7), whereas collapsed globular structures were observed for native PolyA (Figure 2C). These results complement the spectroscopic data and confirm that non-covalent interactions between the peptide–nucleotide side-chains led to a lateral alignment and to more extended conformations. Synchrotron small angle X-ray scattering (SAXS) revealed similar scattering curves for the artificial RNA and DNA homopolymers with only slight differences with respect to the control polypeptide pAAGT and native RNA (SI, Figure S8). The scattering profiles were all straight and featureless with a slope of –1.60 for the artificial homopolymers, compared to –1.45 for the control polypeptide, pAAGT. A negative slope of –1 is indicative of cylinders. After fitting the data using a flexible cylinder model, the cross-sectional diameter for both artificial RNA and DNA polymers were calculated to be ~3.6 nm, in contrast to 3.0 nm for pAAGT (SI, Table S1). These values agree with the fibre diameter of ~4 nm observed in TEM (Figure 2A and B).

Additionally, dynamic nuclear polarization (DNP)-enhanced ^{31}P dephased ^{15}N observed rotational-echo double-resonance (REDOR) experiments[35] were performed on selected samples. This solid-state NMR technique extracts information about the distance between the nitrogen atoms of the amino acids and nucleotide relative to the phosphorous atom of the phosphate group, thereby allowing the investigation of the conformation, hence folding, of the nucleobase relative to the peptide linker. As a model homopolymer, pAAGT-dT was used as pAAGT-rA was insufficient (only ~5 mg was used instead of the required ~10 mg) to obtain a reliable signal enhancement. A significant DNP signal enhancement (ε^{DNP}) of 94 with a build-up time T_B of 3.4 s was obtained, upon which each ^{15}N signals at natural abundance were observed. pAAGT-dT (SI, Figure S9A) showed the expected peaks correlating to glycine and threonine (centred at 109 ppm) and alanine (at *ca.* 121 ppm) within the peptide linker and N1 (144 ppm) and N3 (154 ppm) of the thymine nucleobase.[36] The Boltzmann-statistic fitting of the REDOR dephasing curves (BS-REDOR)[37] afforded the measurement of distances between the phosphorous and nitrogen atoms (SI, Figure S9B-E) and were determined to be around 7.5 Å (Gly/Thr), 5.8 Å (N1) and 6.5 Å (N3). It is noteworthy that the ^{15}N signal of alanine was not significantly dephased, suggesting that the phosphate group was farther than 10 Å, which is the upper ^{31}P-^{15}N detection limit in the BS-REDOR analysis. This indicates that the pendant peptide-mononucleotide groups are mostly in a stretched configuration rather than backfolded, with the nucleobase facing outwards. This is desired since the mononucleotides should be exposed for complementary binding.

All-atom molecular dynamics simulations were performed on the pAAGT-rA and pAAGT-rU homopolymers to obtain detailed atomistic insights into their structural packing and conformation. Homopolymers containing 32 grafted (32-mer) adenine or uracil modified peptide side-chains (pAAGT-rA_{32} and pAAGT-rU_{32}) were placed in a simulation box and simulated in explicit solvent commensurate to experimental conditions. Clustering analysis, used to determine the most favorable structures, showed that both pAAGT-rA_{32} and pAAGT-rU_{32} polymers adopted unfolded backbone conformations (Figure 3A). The pAAGT-rA_{32} polymer produced 65 clusters in total, where the most populated cluster contained 24% of the sampled

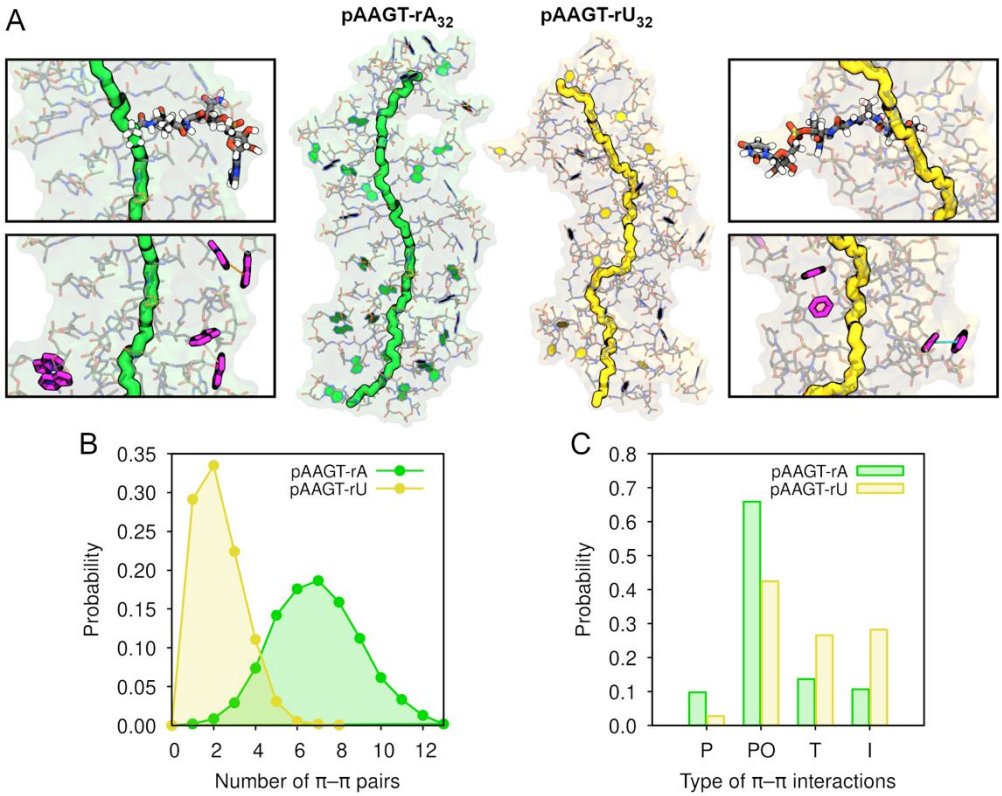

Figure 3. Molecular dynamics simulations of a 32-mer pAAGT-rA ($pAAGT_{32}$, backbone in green) or pAAGT-rU ($pAAGT_{32}$, backbone in yellow) showed unfolded fibre-like morphologies (A). Nucleobase stacking by π-π interactions was evident for pAAGT-rA_{32} in the form of dimers up to tetramers (π-π pairs shown in purple), however, were significantly less prominent in pAAGT-rU_{32}, indicating higher dynamics within pAAGT-rU polymers (insets left and right, respectively). The peptide-nucleotide side-chains are highlighted based on the atom distribution (grey (C), blue (N), red (O), mustard (P)), with the nucleobase rings filled in green (adenine) and yellow (uracil), respectively. The hydrogens were excluded for clarity. A typical peptide side-chain conformation in each polymer is shown as inset in all-atom resolution. The existence of more π-π interactions in pAAGT-rA_{32} was evident from the probability distribution plots of the number of π-π pairs (B) and the most prominent type of π-π stacking was parallel offset (C); P (parallel), PO (parallel offset), T (T-edge) and I (intermediate).

population. In contrast, a total of 89 clusters and 18% population of the most frequently sampled cluster was obtained for pAAGT-rU_{32} (SI, Figure S10), indicating more structural variations, and hence higher dynamics, which was also apparent from the average root mean square fluctuations (SI, Figure S11). Representative structures of the most populated clusters of each polymer are shown in Figure 3A, which exhibit an unfolded fibre-like morphology, in agreement with the structures observed in TEM (Figure 2A). Furthermore, the approximate cross-sectional cylindrical radius of the polymer was estimated by using the lateral atom number density profile along the XY-plane (width) of the homopolymer (with the Z-axis being the molecular axis). Both the pAAGT-rA_{32} and pAAGT-rU_{32} polymers exhibited a diameter of ~3.4 nm (Table S2). This agrees with the flexible cylindrical shape determined from the SAXS data (SI, Figure S8 and Table S1).

The structures contained within the most populated cluster were further interrogated to elucidate the side-chain arrangement and interactions of the preferred polymer conformation. The pAAGT-rA_{32} polymer was stabilized by persistent π–π stacking between the nucleotides (Figure 3B), with adenine moieties stacking in dimers up to tetramers, in which the latter contains a parallel-offset π–π stacking arrangement (Figure 3A and C). The presence of dimeric adenine interactions rather than extended stacking could explain the gradual differences seen in the CD upon increasing temperature (Figure 1A). The uracil nucleotides in pAAGT-rU_{32} experienced very little stacking (Figure 3B) and were more mobile and solvent exposed compared to the adenines (SI, Figure S11). This supports the CD results (SI, Figure S4) in which pAAGT-rU (and native polyU) were shown to be stable upon increasing temperature, which suggested negligible interactions between the uracil nucleotides.

The non-covalent interactions between the peptide chains were closely examined within the central 16-mer core where the polymer showed the highest stability. The distance between the phosphate and glycine's amine within the peptide linker (P–Gly), as well as between phosphate and the N1 and N3 atoms of adenine and uracil nucleobases (P–N1 and P–N3, respectively) were calculated to determine side-chain arrangements (SI, Table S2). The simulations showed average distances of 7.3 Å (rA) and 7.4 Å (rU) for P–Gly; 8.3 Å (rA) and 5.6 Å (rU) for P–N1; and 7.1 Å (rA) and 7.3 Å (rU) for P–N3, which are in agreement with respect to the REDOR NMR data for the model pAAGT-dT polymer (7.5, 5.8 and 6.5 Å, respectively). The maximum P–

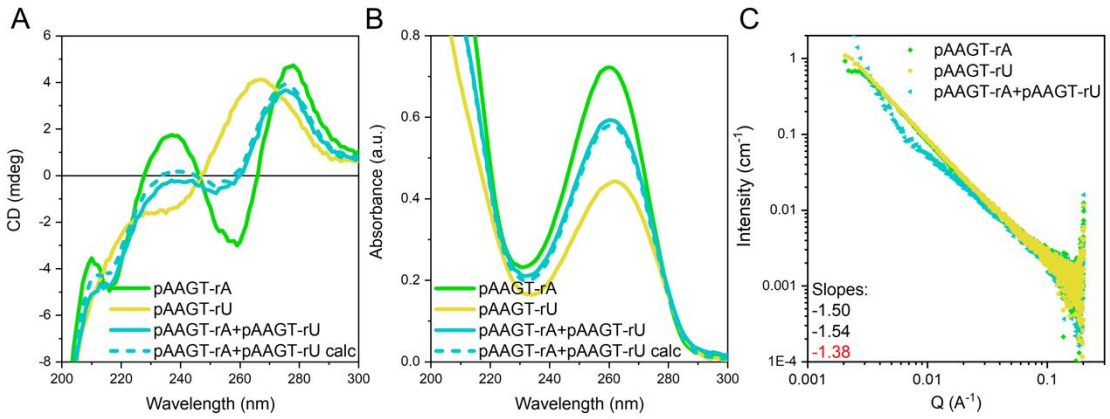

Figure 4. CD (A), UV (B) and SAXS (C) spectra of artificial homopolymer pAAGT-rA (green), pAAGT-rU (yellow) and the combination of the two polymers, pAAGT-rA+pAAGT-rU (turquoise) in 10 mM phosphate buffer with 100 mM NaCl. Slight differences were observed between the spectra for the two polymers and the sum of the two individual spectra (dashed lines) indicating potential complementary binding. c_{Total} = 0.35 mg mL^{-1} (A and B) or 2 mg mL^{-1} (C).

N (amine) distance measured for alanine within single side-chains was 11.9 Å and 11.6 Å for pAAGT-rA_{32} and pAAGT-rU_{32}, respectively, demonstrating an elongated peptide side-chain conformation (also evident in the insets of Figure 3A). Hydrogen bond analysis showed minimal interactions of the hydroxyl groups between lateral riboses, however, are more prominent between amides arising from the peptide moieties. The average total number of hydrogen bonds for both polymers were similar (SI, Table S2).

Elucidating complementary binding between mixed homopolymers. The ability of the artificial nucleic acid polymers to engage in complementary binding (adenine with uracil or thymine) was investigated. The "Oligo Analyzer Tool" of Integrated DNA Technologies[38] which uses a nearest-neighbour analysis.[39] was utilized to calculate melting temperatures and gain an understanding of the expected binding strengths for similar, yet naturally, derived homo-oligonucleotides. This tool revealed that at a 5 µM oligonucleotide concentration supplemented with 100 mM NaCl, a sequence length of at least 10 adenines (A_{10}) with the same length of complementary thymines (T_{10}) is necessary to yield a double stranded melting temperature of around room temperature (SI, Table S3). The binding of these complementary homonucleotides is inherently weak which is reduced even further when there is a mismatch in the antiparallel alignment, as may occur in incorrect spacing between the nucleotides due to, *e.g.*, point insertions and dilutions, thereby distorting optimal intermolecular nucleotide-nucleotide alignment. Despite the low binding strength, we further investigated whether complementary binding, both with its corresponding artificial variant and native RNA or DNA, was still possible.

Firstly, CD and UV spectra of the artificial complementary pairs were recorded and compared against the sum of the individual spectra (SI, Figure S10), that is, the theoretical expected spectra where no or negligible interactions are assumed (denoted as calc). The RNA mimicking polymers pAAGT-rA and pAAGT-rU were investigated in detail as these displayed the highest CD signal and potentially the most ordered conformation. Very small differences between the theoretically calculated spectra of the individual polymers and the experimentally acquired spectra of the mixtures were observed in both CD and UV spectroscopy (Figure 4A-B, and SI, Figure S12, top). The overall CD signal appeared slightly reduced, while the UV absorbance at 260 nm appeared slightly increased. This might hint to weak and transient interactions even though double stranded DNA typically shows a reduction in UV absorbance, due to hypochromic shielding of the nucleobases from UV absorption, not an increase in absorbance. An increase in UV signal might suggest bundling and/or intercalation due to hydrophobic effects and π–π interactions, and to a lesser extent by traditional hydrogen bonding between base pairs. The presence of impurities might also affect the binding kinetics, as well as a mismatch in (anti)parallel alignment. The highly dynamic interactions arising from too few binding events present at the same time might therefore not be detectable using UV and CD spectroscopy. Molecular dynamics simulations of mixed pAAGT-rA_{32} and pAAGT-rU_{32} polymers showed spontaneous but transient binding between the polymers (SI, Figure S13). The association between the complementary polymers was stabilized predominantly by hydrophobic and π–π interactions between the pendant nucleobases, demonstrating weak hybridization. Similarly, small differences were observed in both CD and UV spectra upon mixing pAAGT-rA with native PolyU (SI, Figure S12, middle) and pAAGT-rU mixed with native PolyA (SI, Figure S12, bottom).

Potential complementary binding was more evident from SAXS experiments, in which the mixture of pAAGT-rA with pAAGT-rU displayed a deviated scattering curve with an altered slope of –1.38 instead of approximately –1.50 (Figure 4C), indicating differences in morphology. Similarly, differences in the slope and shape of the SAXS curves of the other mixed variants were also observed (SI, Figure S14). Although the scattering curves indicated a higher polydispersity and the existence of different species (high variation at low Q, and two slopes), which makes

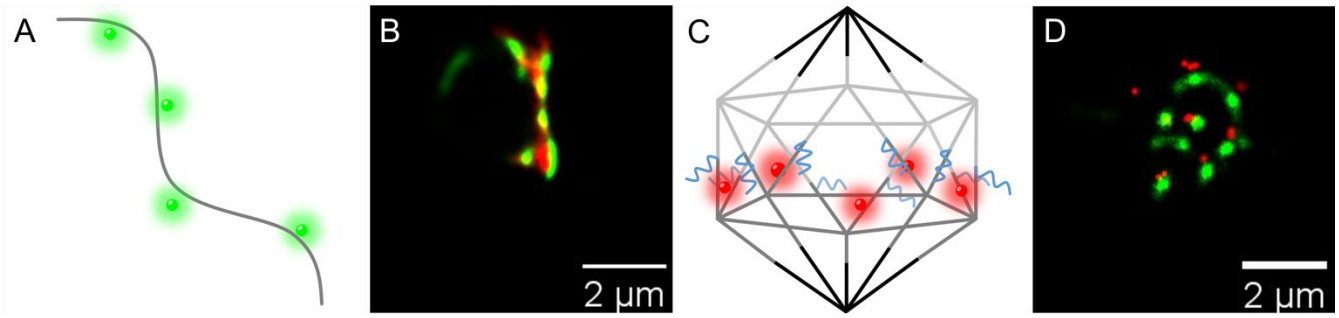

Figure 5. Cartoon representations of a dye-labelled pAAGT-rA polymer (A) and DNA icosahedron (C), and the complementary binding of pAAGT-rA to pAAGT-rU (B), and of pAAGT-rA to DNA icosahedra (D) as revealed by super resolution microscopy (dSTORM). Sulfo-cy3 functionalized pAAGT-rA polymer (green, A for a cartoon representation and B for a dSTORM image) intertwined with a pAAGT-rU polymer (red, B), whereas DNA icosahedra (red, C for a cartoon representation and D for a dSTORM image) aligned next to a sulfo-cy3 functionalized pAAGT-rA polymer (green). The DNA icosahedron was decorated with five sulfo-cy5 labels (red) and designed to contain 10 pendant T-sequences (T_{10}, highlighted in blue, C), to allow complementary binding to the pAAGT-rA scaffold. The dimensions of the DNA icosahedron are approximately 20 nm × 20 nm and the different 5-way junctions making up the DNA icosahedron are indicated in black (2×), light grey (5×) and dark grey (5×) lines, with the centre of the 5-junctions being positioned at the corners of the structure (C). For dSTORM imaging (B and D) a concentration of 0.17 mg mL^{-1} (artificial RNA) was used.

interpretation and data fitting more challenging and less reliable, both the radii and flexibility (*i.e.*, the Kuhn length) seemed to be altered (Table S4, note that the low Q range did not fit well with the flexible cylinder model). Similarly, small-angle neutron scattering (SANS) measurements of the mixed samples showed a shoulder at higher Q values, which was absent in the individual samples (SI, Figure S15). Taken together, these results suggest the existence of complementary binding, though, considering the small differences, this complementary binding might be transient and dynamic rather than fixed, as also seen from the modelling simulations data.

Visualizing mixed samples revealed complementary interactions. Atomic force microscopy (AFM) and direct stochastic optical reconstruction microscopy (dSTORM) were employed to visualize and investigate the potential binding of the mixed samples, pAAGT-rA+pAAGT-rU, and to rule out any influence that might have occurred as a consequence of nucleotide remnants. Compared to the individual homopolymers, altered height profiles were observed for the mixed samples in dry AFM (SI, Figure S16) suggesting the existence of specific or non-specific interactions.

Upon mixing 5 mol% sulfo-cy3 (green) functionalized pAAGT-rA (see Figure 5A for a cartoon representation, and SI, Figure S17, left for the molecular structure and dSTORM representative image) and 5 mol% sulfo-cy5 (red) functionalized pAAGT-rU (SI, Figure S17, right), dSTORM revealed the existence of intertwined polymers (Figure 5B). These observations provide evidence for complementary binding. In contrast, Föster resonance energy transfer (FRET) between the FRET-pair labelled homopolymers was low (SI, Figure S18), indicating the absence of close proximity (<10 nm) of the donor (sulfo-cy3 in pAAGT-rA) and acceptor (sulfo-cy5 in pAAGT-rU). This might be due to the location of the dyes, as the FRET dyes were installed directly at the C-terminus of the peptide linker, rather than on the mononucleotides themselves. The absence of a sufficient hydrophobic pocket and the high-water solubility of the sulfo-dyes may also reduce efficient energy transfer. Additionally, the intrinsic tendency of the dyes to aggregate (*i.e.*, form aggregated blocks) upon increased temperature (necessary to form the dye-labelled co-polymers), might also have quenched energy transfer. Blocky dye segments were observed in dSTORM images, confirming the existence of cy3 or cy5 blocks within the structures rather than a homogeneous distribution.

Small changes in morphology appearance were also observed under TEM (SI, Figure S19). Weak binding was also seen in the isothermal titration calorimetry (ITC), which measures binding strengths from the heat generation of titrated ligands. Only a gradual change in the binding isotherm (shallow slope) was observed in the ITC when titrating pAAGT-rU to a 20-mer adenine oligonucleotide (SI, Figure S20), rather than a cooperative binding (S-curve) normally observed in receptor-ligand binding.[40]

In addition, a three-dimensional DNA-folded structure, with multivalent pendent toeholds was designed to investigate whether it could hybridize to the complementary artificial RNA polymer pAAGT-rA. Previously designed spherical, *i.e.*, icosahedral,[41, 42] DNA-folded structures (~20 nm × 20 nm) were adapted to contain 10 pendant oligonucleotides (T_{10}) facing out of the folded structure (Figure 5C, blue lines) serving as toeholds that can interact with the long artificial template pAAGT-rA (Figure 5A).

The DNA icosahedron, containing the toeholds on the top half, and cy5-functionalized oligonucleotide strands on the bottom half (SI, Table S5), was assembled using a 3-step protocol (SI, Figure S21, left). First, the staple strands that make up the building blocks of the icosahedron, *i.e.*, 5-way junctions, were separately assembled using slow thermal annealing from 80 °C to 20 °C. In the second step, the top and bottom halves of the icosahedron were assembled separately by isothermal annealing at 30 °C, followed by the formation of the full icosahedron through combining the top and bottom halves and annealing at 30 °C. The different steps in DNA folding were characterized using agarose gel

electrophoresis (SI, Figure S21, right). Subsequently, the folded icosahedron solution was mixed with a sulfo-cy3 functionalized pAAGT-rA scaffold and investigated using dSTORM. Under super resolution microscopy, the artificial scaffold (green) seemed to wrap around the icosahedron structures (red), even after the scaffold was first adhered to the coverslip before the icosahedron was added (Figure 5D). This suggests that the complementary binding, arguably increased by multivalent interactions, is stronger than the adhesive forces onto the coverslip.

Likewise, a more rigid, DNA origami barrel structure (30 × 27 nm),[43] was adapted to contain 20 oligoadenine (A_{20}) sequences facing out of the structure, to investigate complementary binding to artificial pAAGT-rU. Origami barrels were folded as previously reported[43, 44] and purified by agarose gel electrophoresis prior to mixing with pAAGT-rU. After annealing the mixture at room temperature for about 68 hours in the presence of 10 mM $MgCl_2$, complementary binding was evaluated using TEM. DNA origami barrel structures were observed that were located next to and on top of pAAGT-rU bundled fibers, a large portion of unbound barrels was also observed (SI, Figure S22). This observation supplements the above findings; complementary binding events are evident, however, are weak and transient, and hence highly dynamic. Nevertheless, these results demonstrate that RNA mimicking polymers can interact with both native RNA and DNA, and be used to construct larger (functional) structures.

CONCLUSIONS

Here, a modular synthesis platform for the fabrication of novel RNA and DNA polypeptide polymers was developed and characterized using experimental and computational modelling techniques. The incorporation of a peptide linker between the polymer backbone (polymethacrylate) and the mononucleotides ensured an unfolded conformation of the polymers due to predesigned lateral non-covalent interactions. By merging the design principles of polymer science and supramolecular chemistry, successful fibrous single stranded homopolymers could be assembled where the mononucleotide side-chains were exposed at their periphery, allowing for complementary binding. Despite the lack of structural diversity (*i.e.*, containing all 4 nucleotides) within the polymer, which dramatically reduced binding strengths, complementary binding was demonstrated upon combining both single stranded polymers (artificial and native) and more complex 3D DNA folded structures. The established modular synthesis pathway can be further extended to fabricate random and block-copolymers with various sequences of extended lengths. These polymers open up opportunities to be employed as templates for the large-scale synthesis of both artificial and natural nucleic acids (*e.g.*, by non-enzymatic primer extension reactions) and for various biomedical applications, including biosensing and gene delivery.

ASSOCIATED CONTENT

Supporting Information.

Additional information concerning the materials and instrumentation used, synthetic procedures including proton and phosphorous NMR, and additional Figures can be found in the supporting information. This material is available free of charge *via* the Internet at http://pubs.acs.org.

AUTHOR INFORMATION

Corresponding Author

* Simone I.S. Hendrikse, shendriksela@unimelb.edu.au, Amanda V. Ellis, amanda.ellis@unimelb.edu.au.

Author Contributions

All authors have given approval to the final version of the manuscript.

Funding Sources

This work was supported by funding from the Australian Research Council (ARC), Discovery Projects to A.V.E. (DP190100055), A.C.F (DP210102133) and P.T. (DP190101892), the McKenzie Fellowship from the University of Melbourne to S.I.S.H, and Australian Nanotechnology Network.

ACKNOWLEDGMENTS

SAXS experiments were performed on the SAXS/WAXS beamline and SANS experiments on the Bilby small angle neutron scattering beamline of the Australian Synchrotron, ANSTO. The authors thank Dr. Nigel Kirby and Dr. Timothy Ryan for support during the SAXS experiments, and Dr. Andrew Whitten for performing the SANS measurements. Prof. Eric Hanssen and Sepideh Valimehr from the Ian Holmes Imaging Center are acknowledged for TEM measurements, the Melbourne protein characterization platform, the Mass Spectrometry and Proteomics Facility at the University of Melbourne, and the Katharina Gaus Light Microscopy Facility at UNSW for instrument maintenance. Access to NMR and DNP NMR spectrometers was provided by the Bio21 Institute at the University of Melbourne. The computational modelling work was supported by HPC resources provided by the Australian Government through the National Computational Infrastructure Project (e90). Finally, we thank the group of E.W. Meijer at the Eindhoven University of Technology for additional instrumentation support.

REFERENCES

(1) Alberts, B.; Johnson, A.; Lewis, J., The Structure and Function of DNA. In *Molecular Biology of the Cell*, 4th edition ed.; Garland Science: New York, 2002.
(2) Breaker, Ronald R.; Joyce, Gerald F., The Expanding View of RNA and DNA Function. *Chemistry & Biology* **2014,** *21* (9), 1059-1065.
(3) Alberts, B.; Johnson, A.; Lewis, J., From DNA to RNA. In *Molecular Biology of the Cell*, 4th edition ed.; Garland Science: New York, 2002.
(4) Dykstra, P. B.; Kaplan, M.; Smolke, C. D., Engineering synthetic RNA devices for cell control. *Nature Reviews Genetics* **2022,** *23* (4), 215-228.
(5) Roh, Y. H.; Ruiz, R. C. H.; Peng, S.; Lee, J. B.; Luo, D., Engineering DNA-based functional materials. *Chem. Soc. Rev.* **2011,** *40* (12), 5730-5744.
(6) Duffy, K.; Arangundy-Franklin, S.; Holliger, P., Modified nucleic acids: replication, evolution, and next-generation therapeutics. *BMC Biology* **2020,** *18* (1), 112.
(7) Hendrikse, S. I. S.; Gras, S. L.; Ellis, A. V., Opportunities and Challenges in DNA-Hybrid Nanomaterials. *ACS Nano* **2019,** *13* (8), 8512-8516.

(8) Chen, T.; Hongdilokkul, N.; Liu, Z.; Thirunavukarasu, D.; Romesberg, F. E., The expanding world of DNA and RNA. *Current Opinion in Chemical Biology* **2016,** *34*, 80-87.
(9) Whitfield, C. J.; Zhang, M.; Winterwerber, P.; Wu, Y.; Ng, D. Y. W.; Weil, T., Functional DNA–Polymer Conjugates. *Chem. Rev.* **2021,** *121* (18), 11030-11084.
(10) Ziach, K.; Chollet, C.; Parissi, V.; Prabhakaran, P.; Marchivie, M.; Corvaglia, V.; Bose, P. P.; Laxmi-Reddy, K.; Godde, F.; Schmitter, J.-M.; Chaignepain, S.; Pourquier, P.; Huc, I., Single helically folded aromatic oligoamides that mimic the charge surface of double-stranded B-DNA. *Nat. Chem.* **2018,** *10* (5), 511-518.
(11) Yang, H.; Xi, W., Nucleobase-Containing Polymers: Structure, Synthesis, and Applications. *Polymers* **2017,** *9* (12), 666.
(12) Gupta, A.; Mishra, A.; Puri, N., Peptide nucleic acids: Advanced tools for biomedical applications. *Journal of Biotechnology* **2017,** *259*, 148-159.
(13) Quijano, E.; Bahal, R.; Ricciardi, A.; Saltzman, W. M.; Glazer, P. M., Therapeutic Peptide Nucleic Acids: Principles, Limitations, and Opportunities. *The Yale journal of biology and medicine* **2017,** *90* (4), 583-598.
(14) Sahu, B.; Sacui, I.; Rapireddy, S.; Zanotti, K. J.; Bahal, R.; Armitage, B. A.; Ly, D. H., Synthesis and Characterization of Conformationally Preorganized, (R)-Diethylene Glycol-Containing γ-Peptide Nucleic Acids with Superior Hybridization Properties and Water Solubility. *The Journal of Organic Chemistry* **2011,** *76* (14), 5614-5627.
(15) Ellington, A.; Pollard Jr., J. D., Introduction to the Synthesis and Purification of Oligonucleotides. *Current Protocols in Nucleic Acid Chemistry* **2000,** *00* (1), A.3C.1-A.3C.22.
(16) Braasch, D. A.; Nulf, C. J.; Corey, D. R., Synthesis and Purification of Peptide Nucleic Acids. *Current Protocols in Nucleic Acid Chemistry* **2002,** *9* (1), 4.11.1-4.11.18.
(17) Sun, H.; Yang, L.; Thompson, M. P.; Schara, S.; Cao, W.; Choi, W.; Hu, Z.; Zang, N.; Tan, W.; Gianneschi, N. C., Recent Advances in Amphiphilic Polymer–Oligonucleotide Nanomaterials via Living/Controlled Polymerization Technologies. *Bioconjugate Chem.* **2019,** *30* (7), 1889-1904.
(18) Doncom, K. E. B.; Blackman, L. D.; Wright, D. B.; Gibson, M. I.; O'Reilly, R. K., Dispersity effects in polymer self-assemblies: a matter of hierarchical control. *Chem. Soc. Rev.* **2017,** *46* (14), 4119-4134.
(19) Liu, K.; Zheng, L.; Liu, Q.; de Vries, J. W.; Gerasimov, J. Y.; Herrmann, A., Nucleic Acid Chemistry in the Organic Phase: From Functionalized Oligonucleotides to DNA Side Chain Polymers. *J. Am. Chem. Soc.* **2014,** *136* (40), 14255-14262.
(20) Dore, M. D.; Trinh, T.; Zorman, M.; de Rochambeau, D.; Platnich, C. M.; Xu, P.; Luo, X.; Remington, J. M.; Toader, V.; Cosa, G.; Li, J.; Sleiman, H. F., Thermosetting supramolecular polymerization of compartmentalized DNA fibers with stereo sequence and length control. *Chem* **2021,** *7* (9), 2395-2414.
(21) Rizzuto, F. J.; Dore, M. D.; Rafique, M. G.; Luo, X.; Sleiman, H. F., DNA Sequence and Length Dictate the Assembly of Nucleic Acid Block Copolymers. *J. Am. Chem. Soc.* **2022,** *144* (27), 12272-12279.
(22) Roloff, A.; Nelles, D. A.; Thompson, M. P.; Yeo, G. W.; Gianneschi, N. C., Self-Transfecting Micellar RNA: Modulating Nanoparticle Cell Interactions via High Density Display of Small Molecule Ligands on Micelle Coronas. *Bioconjugate Chem.* **2018,** *29* (1), 126-135.
(23) Peng, L.; Wu, C. S.; You, M.; Han, D.; Chen, Y.; Fu, T.; Ye, M.; Tan, W., Engineering and applications of DNA-grafted polymer materials. *Chem. Sci.* **2013,** *4* (5), 1928-1938.
(24) Grubbs, R. B.; Grubbs, R. H., 50th Anniversary Perspective: Living Polymerization—Emphasizing the Molecule in Macromolecules. *Macromolecules* **2017,** *50* (18), 6979-6997.
(25) Corrigan, N.; Jung, K.; Moad, G.; Hawker, C. J.; Matyjaszewski, K.; Boyer, C., Reversible-deactivation radical polymerization (Controlled/living radical polymerization): From discovery to materials design and applications. *Progress in Polymer Science* **2020,** *111*, 101311.
(26) Mahler, A.; Reches, M.; Rechter, M.; Cohen, S.; Gazit, E., Rigid, Self-Assembled Hydrogel Composed of a Modified Aromatic Dipeptide. *Advanced Materials* **2006,** *18* (11), 1365-1370.
(27) Gray, D. M.; Hung, S.-H.; Johnson, K. H., [3] Absorption and circular dichroism spectroscopy of nucleic acid duplexes and triplexes. In *Methods in Enzymology*, Academic Press: 1995; Vol. 246, pp 19-34.
(28) Gody, G.; Maschmeyer, T.; Zetterlund, P. B.; Perrier, S., Rapid and quantitative one-pot synthesis of sequence-controlled polymers by radical polymerization. *Nature Communications* **2013,** *4* (1), 2505.
(29) Abou Assi, H.; Garavís, M.; González, C.; Damha, M. J., i-Motif DNA: structural features and significance to cell biology. *Nucleic Acids Research* **2018,** *46* (16), 8038-8056.
(30) Spiegel, J.; Adhikari, S.; Balasubramanian, S., The Structure and Function of DNA G-Quadruplexes. *Trends in Chemistry* **2020,** *2* (2), 123-136.
(31) Dodero, V. I.; Quirolo, Z. B.; Sequeira, M. A., Biomolecular studies by circular dichroism. *FBL* **2011,** *16* (1), 61-73.
(32) Schweitzer-Stenner, R. Soffer, J.B. 1.23 Optical Spectroscopy, Comprehensive Biophysics, *Elsevier* **2012**, 533-559.
(33) Hendrikse, S. I. S.; Su, L.; Hogervorst, T. P.; Lafleur, R. P. M.; Lou, X.; van der Marel, G. A.; Codee, J. D. C.; Meijer, E. W., Elucidating the Ordering in Self-Assembled Glycocalyx Mimicking Supramolecular Copolymers in Water. *J. Am. Chem. Soc.* **2019,** *141* (35), 13877-13886.
(34) Higashi, S. L.; Ikeda, M., Development of an Amino Sugar-Based Supramolecular Hydrogelator with Reduction Responsiveness. *JACS Au* **2021,** *1* (10), 1639-1646.
(35) Greenwood, A. I.; Clay, M. C.; Rienstra, C. M., 31P-dephased, 13C-detected REDOR for NMR crystallography at natural isotopic abundance. *Journal of Magnetic Resonance* **2017,** *278*, 8-17.
(36) Separovic, F.; Hofferek, V.; Duff, A. P.; McConville, M. J.; Sani, M.-A., In-cell DNP NMR reveals multiple targeting effect of antimicrobial peptide. *Journal of Structural Biology: X* **2022,** *6*, 100074.
(37) Gehman, J. D.; Separovic, F.; Lu, K.; Mehta, A. K., Boltzmann Statistics Rotational-Echo Double-Resonance Analysis. *The Journal of Physical Chemistry B* **2007,** *111* (27), 7802-7811.
(38) OligoAnalyzer™ Tool. idtdna.com.
(39) Allawi, H.T. and SantaLucia, J. Thermodynamics and NMR of Internal G·T Mismatches in DNA. *Biochemistry* **1997**, 36 (34), 10581-10594.
(40) Velazquez-Campoy, A.; Goñi, G.; Peregrina, J. R.; Medina, M., Exact Analysis of Heterotropic Interactions in Proteins: Characterization of Cooperative Ligand Binding by Isothermal Titration Calorimetry. *Biophysical Journal* **2006,** *91* (5), 1887-1904.
(41) Bhatia, D.; Mehtab, S.; Krishnan, R.; Indi, S. S.; Basu, A.; Krishnan, Y., Icosahedral DNA Nanocapsules by Modular Assembly. *Angew. Chem., Int. Ed.* **2009,** *48* (23), 4134-4137.
(42) Banerjee, A.; Bhatia, D.; Saminathan, A.; Chakraborty, S.; Kar, S.; Krishnan, Y., Controlled Release of Encapsulated Cargo from a DNA Icosahedron using a Chemical Trigger. *Angew. Chem., Int. Ed.* **2013,** *52* (27), 6854-6857.
(43) Wickham, S. F. J.; Auer, A.; Min, J.; Ponnuswamy, N.; Woehrstein, J. B.; Schueder, F.; Strauss, M. T.; Schnitzbauer, J.; Nathwani, B.; Zhao, Z.; Perrault, S. D.; Hahn, J.; Lee, S.; Bastings, M. M.; Helmig, S. W.; Kodal, A. L.; Yin, P.; Jungmann, R.; Shih, W. M., Complex multicomponent patterns rendered on a 3D DNA-barrel pegboard. *Nature Communications* **2020,** *11* (1), 5768.
(44) Daljit Singh, J. K.; Luu, M. T.; Berengut, J. F.; Abbas, A.; Baker, M. A. B.; Wickham, S. F. J., Minimizing Cholesterol-Induced Aggregation of Membrane-Interacting DNA Origami Nanostructures. *Membranes* **2021,** *11* (12), 950.

Insert Table of Contents artwork here

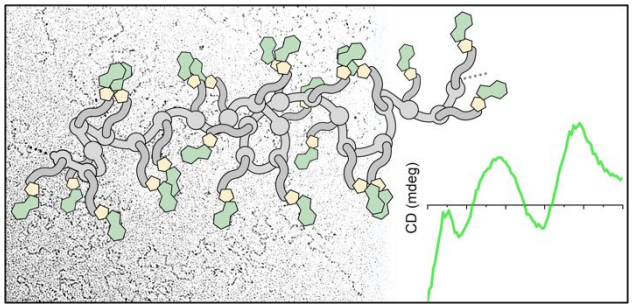
CD (mdeg)